Master of Science

EXPERIMENTAL INVESTIGATION OF FRICTIONAL PROPERTIES OF TWO-DIMENSIONAL HYBRID ORGANIC-INORGANIC PEROVSKITES

The Graduation School of the University of Ulsan

School of Mechanical Engineering

Van Vo Kim Hieu

EXPERIMENTAL INVESTIGATION OF FRICTIONAL PROPERTIES OF TWO-DIMENSIONAL HYBRID ORGANIC-INORGANIC PEROVSKITES

Supervisor: Professor **Koo-Hyun Chung**

A Thesis

Submitted to the Graduate School of the University of Ulsan

in Partial Fulfillment of the Requirements

for the Degree of Master of Science

by

Van Vo Kim Hieu

School of Mechanical Engineering

University of Ulsan, Republic of Korea

May 2022

EXPERIMENTAL INVESTIGATION OF FRICTIONAL PROPERTIES OF TWO-DIMENSIONAL HYBRID ORGANIC-INORGANIC PEROVSKITES

This certifies that the master's thesis

of **Van Vo Kim Hieu** is approved.

Committee Chairman:	Prof. Doo-Man Chun
Committee Member:	Prof. Koo-Hyun Chung
Committee Member:	Prof. Yoon-Ho Lee

School of Mechanical Engineering

University of Ulsan, Republic of Korea

June 2022

ACKNOWLEDGEMENTS

Firstly, I would like to express my sincere and deep gratitude to my advisor, Professor Koo-Hyun Chung, for his support, encouragement, and guidance throughout this research. He taught me how to think deeply and gave me a lot of advice on research to do better. From my bottom heart, he is a person who gives me the chance to study abroad and fulfill my dreams. Without his kind-hearted support, I would not have been the present results.

And I am very grateful for the guidance and support of all my laboratory members (Tribology and Surface Engineering Laboratory, University of Ulsan) when I have a hard time working.

Finally, a great thanks to my family and friends who always being there to caring and encourage me, which is my great driving force in implementing this thesis.

ABSTRACT

Two-dimensional (2D) hybrid organic-inorganic perovskites (HOIPs) have attracted remarkable attention over the years because of their outstanding physical properties for application in optoelectronic devices. 2D HOIPs have been proposed as the next generation materials for solar-collecting applications as well as light-emitting diodes, due to the higher moisture and illumination stability. Recently, extensive efforts have been made to understand the properties of 2D HOIPs. As a result, it was found that 2D HOIPs may provide improved electronic properties and environmental stability by using pentylamine as organic spacer molecules between inorganic materials without significantly affecting the optical properties. It was also shown that 2D HOIPs encapsulated hexagonal boron nitride exhibited higher environmental stability. In addition, the photoluminescence of 2D HOIPs was found to be promoted by mixing with polymers. It was further shown that the optical bandgap of the polymer-mixed 2D HOIPs gradually increased with increasing concentration of polymers and that the photoluminescence lifetime increased due to the improved crystalline quality and reduced trapping states. Given that mechanical properties of 2D HOIPs may significantly affect the manufacturing process as well as the durability of devices, mechanical properties such as elasticity and hardness were investigated. Especially, recent studies showed that replacing the organic parts with stiff and multifunctional components may improve the stability of perovskite solar cell absorption and using a specially engineered structure of a thin organic layer can increase elastic modulus and hardness. However, the fundamental frictional properties of 2D HOIPs have not been explored. In this study, the effects of topography, thickness, and organic molecule chain length in HOIPs on friction

were experimentally investigated using atomic force microscopy (AFM). The results showed that the effect of topography on nanoscale friction has been observed according to local slope variation, but the intrinsic friction is low. Also, the thickness-dependent friction behavior and the effect of chain length on the friction characteristics at the nanoscale are significantly smaller than that of the silicon oxide substrate and most clearly observed in single-layer, bi-layer, and bulk films. The findings of this work may be helpful for the performance of 2D HOIPs in various device applications.

TABLE OF CONTENTS

LIST OF FIGURES

1. INTRODUCTION

1.1 Background and motivation

Fossil fuels, being one of the abundant available non-renewal resources, have been exploited over several decades[1]. Although the use of fossil fuels has directly or indirectly enhanced our quality of living, it has several threatening effects on the environment, such as climate change (global warming), rising greenhouse gases (CO_2, CH_4, N_2O & O_3), smog (photochemical & Sulfurous), acidification of the ocean, etc [2, 3]. Besides, the exhaustion of non-renewal resources is to be reduced to maintain sustainable development. Therefore, there is a stipulation to develop an alternative energy source with a trivial environmental impact. Renewable energy sources such as wind, solar, hydro, tidal, geothermal, biomass require serious attention to make them efficient and cost-competitive with traditional energy sources such as coal and petroleum products. Among various renewable sources, solar energy with high abundance has a key role in solving the social, economic, and technological challenges facing human society[3].

In recent years, perovskites are a breakthrough in this field and hybrid organic-inorganic perovskites (HOIPs) based photovoltaic solar cells have attracted great attention due to their direct bandgap electronic properties and higher power conversion efficiencies (Figure 1) [4]. To attain satisfactory environmental stability, the photovoltaic cell must be least reactive to the ambiance changes such as moisture, light, and temperature over a duration of time. However, three-dimensional (3D) HOIPs suffer stability issues, which limits their commercial applicability[5]. Therefore, 2D HOIPs come into the picture, demonstrating a higher conversion efficiency with outstanding properties of absorption, charge-carrying transport, strong luminescence, and easy

fabrication[5]. In addition, 2D HOIPs are applied not only in flexible solar cells but also in wearable sensors and electronic devices such as the indium tin oxide (ITO) flexibility characteristics along with 2D perovskites which can lead to the development of promising flexible nanoelectronics and optoelectronic devices[1, 6].

Extensive efforts have been made to understand frictional behavior, interfacial shear strength, strain effects, in-plane and out-plane mechanical properties, the impact of multiple layers, stretching, and breaking of 2D perovskites. It was explored the vital factors that influence out-of-plane mechanical characteristics of hybrid perovskites, which are significantly affected by the lead halide bond in inorganic (stronger the bond higher Young's modulus), and also demonstrated the interface between organic layers in 2D HOIPs leads to a change in mechanical properties that using a specially engineered structure of thin-layer organic material can lead to higher elastic modulus and hardness value [7]. Besides that, ultra-thin 2D HOIP exhibits superior breaking strength/Young's modulus ratio compared to many other widely used engineering materials and substrates have been shown that the in-plane Young's modulus and breaking strength decrease as thickness increases from single-layer to tri-layer and are almost identical in tri-layer and quad-layer [8]. Besides that, with an increase in the number of inorganic layers in the 2D hybrid halide perovskite, the ductility gradually decreases under the influence of the very large deformation, and it is further deduced that replacing the organic parts with stiff and multifunctional components will lead to improved stability and carrier mobility of perovskite solar cell absorption layer [9]. Another study reports the modulation of the bandgap due to the inducement of strain [10]. When the number of layers increases the strain increases, which can be much higher a 13.3 meV/% for n=5, therefore, the electronic properties of 2D hybrid organic-inorganic perovskites can also be manipulated by strain. Furthermore, the direct shear modulus characterization of the 2D HOIPs perovskites $(C_4H_9NH_3)_2PbBr_4$ in the ⟨001⟩ direction by atomic force microscopy (AFM)

has been reported that the measured shear modulus of 2D perovskite increases significantly with the reduction of atomic layers, especially as the number of layers is less than 60 [11]. Also, it was employed the orientational anisotropic property of the sliding friction for contact-angle-dependent heterojunctions between a 2D single-crystalline hybrid perovskite sheet and ITO [6]. The results revealed that friction depends on the atomic layers in the atomic 2D hybrid perovskite, which first decreases with the increase of the number of layers up to a certain value and then becomes constant. The work done here provides opportunities for the fundamental understanding of tribological properties such as friction and adhesion of atomically thin 2D perovskites which is not well studied for such nanoscale devices.

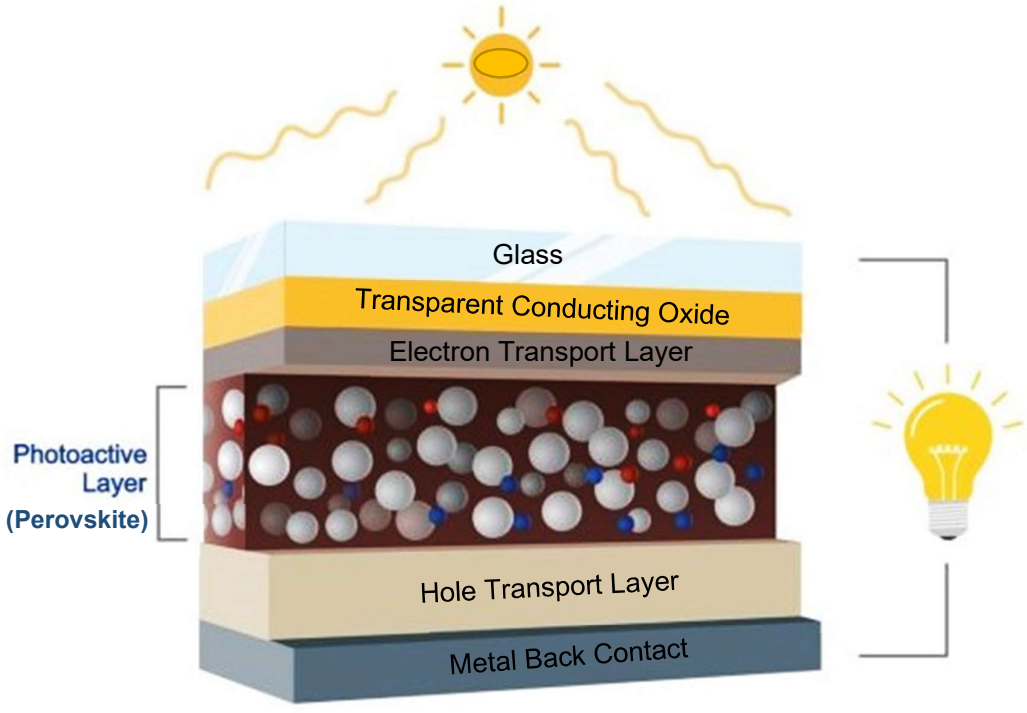

Figure 1. Schematic of the working principle of perovskite cell [4].

1.2 Objective of thesis

This work aims to gain a fundamental understanding on the friction characteristics of atomically thin flakes 2D HOIPs and bulk at the nanoscale. Here, the thickness dependent friction characteristics of 2D HOIPs were quantitative investigated using atomic force microscopy (AFM) under various normal forces to determine the frictional behavior with respect to the organic molecular chain length and the number of layers. Therefore, this work's outcomes might contribute to expanding the applications of 2D HOIPs by suggesting tribological properties that can be tunable through controlling the organic chain length or the number of layers.

1.3 Organization of thesis

The overall structure of this thesis includes four sections, which the motivation and objectives of this work have been explained in section 1.

In section 2, the process of sample preparation and experiment were described. Topographic images from AFM were collected to show the surface morphology as well as cross-sectional height profiles of atomically thin flakes 2D HOIPs and bulk.

In section 3, adhesion and friction behavior obtained from the friction force measurement under various normal forces via contact mode. Then discussion about the effect of organic molecular chain length and number of layers are presented.

Finally, the main conclusions and recommendations of this research are summarized in section 4 for further investigation.

2. EXPERIMENTAL DETAILS

2.1 Sample preparation and characterization

2D Ruddlesden-Popper HOIPs with three different chain lengths were prepared with the general chemical formula of $(C_mH_{2m+1}NH_3)_2(CH_3NH_3)_{n-1}Pb_nI_{3n+1}$, where m and n indicate the number of carbons in the linear organic molecular chain and the number of inorganic layers, respectively. To investigate the effect as the length of the organic spacer molecule changes, the number of inorganic layers was kept at n = 1 and the number of carbons in the organic molecular chain was changed with m = 4, 8, 12, and denoted C4, C8, C12 to represent the types of 2D HOIPs, where the number after C is the number of carbons present in the organic molecular chain.

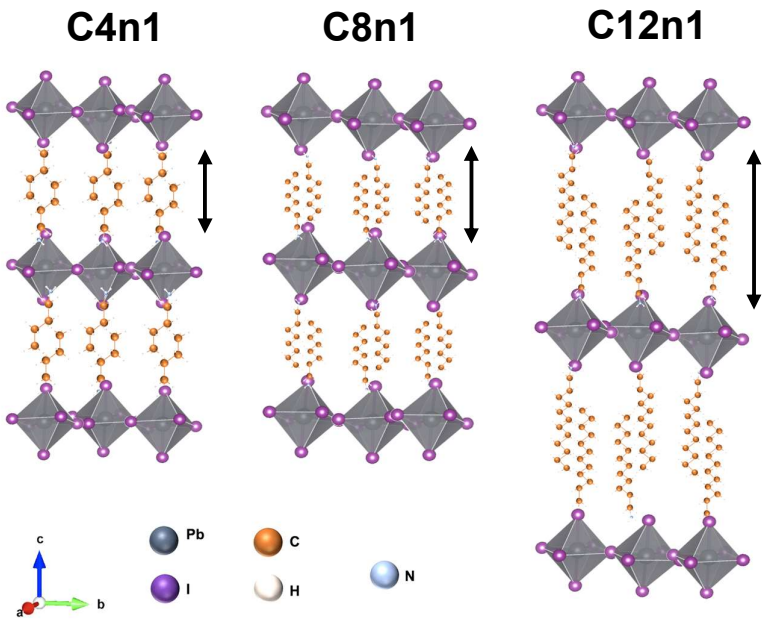

Figure 2. The schematic of the 2D structures of the layered $(C_mH_{2m+1}NH_3)_2(CH_3NH_3)_{n-1}Pb_nI_{3n+1}$ materials with the increasing length of carbons in the organic molecular chain m = 4, 8, and 12 for the same number of inorganic

layers, n = 1. The grey octahedra represent the $[PbI_6]^{4-}$ moieties. The black arrow indicates the increase in the distance of the inorganic layers with increasing the length of the organic spacer.

Due to the presence of the weak Van der Waals interaction between the organic chains of two-unit cells, the synthesized 2D HOIPs crystals were mechanically exfoliated to produce thin flakes of 2D HOIPs and then transferred on a silicon oxide substrate [8, 12]. After that, it was located by using an optical microscope (VK-X200, Keyence) and then imaged surface through AFM (Atomic force microscopy, MFP-3D, Asylum Research) measurement with intermittent contact mode and using a silicon tip (AC240, Olympus) to avoid surface damage.

Figure 3 shows the topographic images and cross-sectional height profiles for C4, C8, and C12 flakes obtained via AFM. The thickness values in the cross-sectional height profiles were averaged over at least three flakes in each case. To determine the thickness of the 2D HOIPs layers must begin with determining that the elemental modular structure is referred to as a "single-layer", which is composed of an inorganic layer and one spacer cation layer [13]. It was found that the thicknesses of the single-layer (1L) sheets for C4, C8, and C12 films were about 1.74, 2.21, and 2.69 nm, respectively. The values are slightly larger than the theoretical values of thin flakes 2D HOIPs [14-16] due to the presence of adhesive residue or absorbed molecules on the substrate [17, 18]. The interlayer spacing values of C4, C8, and C12 were estimated to be about 1.33, 1.76, and 2.11 nm, respectively, which are generally corresponded to their theoretical values and recent reports [12-14, 17], then bi-layer (2L), tri-layer (3L), quad-layer (4L), and bulk flakes were identified.

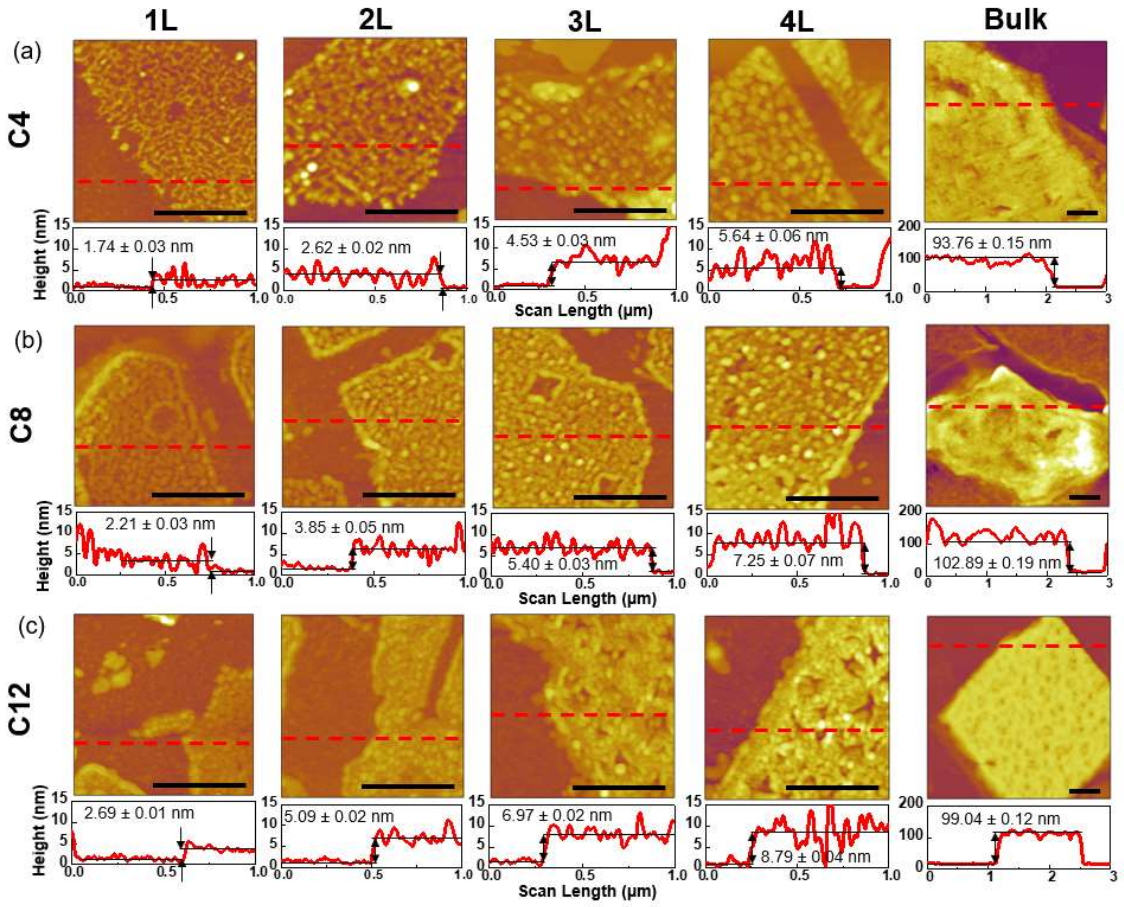

Figure 3. Topographic images of (a) C4, (b) C8, and (c) C12 with single-layer (1L), bilayer (2L), tri-layer (3L), quad-layer (4L), and bulk are measured by AFM. Scale bars, 500 nm. The cross-sectional height profiles are included and the locations are indicated by the red dash lines.

The topographic images showed that the surface morphology of 1L in C4 is rougher than in C8 and C12 which means the number of pinholes on the surface of a single-layer gradually went down as increasing the number of carbon chains from C4 to C12. The same was observed in the topographic images of 2L. Continuing to consider the surface morphology of 2D HOIPs at 3L and 4L, C4 and C12 had a greater number of pinholes on the flakes than C8. Eventually, the number of pinholes of bulk was the most in C12.

These surface morphologies were consistent with the surface roughness average (Ra) values of three types of 2D HOIPs which have been shown in Figure 4. It showed that all C4, C8, and C12 displayed a substantial roughness value compared to the substrate. The surface roughness was found to be increasing with increment in the number of layers, and maximum for the bulk. For a few layers as 1L and 2L, the C4 produced a higher value for the surface roughness, followed by C8 and C12, whereas this trend is opposite for bulk, where the surface roughness is maximum for C12, followed by C8 and C4. Furthermore, the surface roughness of 3L and 4L has the highest values of C4, followed by C12 and then C8. It could be explained that using different short and long organic molecular chains leads to the different morphology's appearance of the three types of 2D HOIPs [19]. In more detail, this roughness might be caused by a local disorder of the organic cations and deformation of the inorganic framework after exfoliation by mechanical stress [20, 21] and related to the interaction between layers [6]. A large number of layers have strong interactions with inner layers and increase the binding energy [6], therefore, after exfoliation, the organic chains that remain at the top and bottom of the inorganic layers could be more disordered and more deformed in the inorganic layers leading to the highest roughness value in bulk. In contrast, the weak interaction of thin layers could less affect the disorder of the remaining organic chains and deformation of the inorganic framework, thus, resulting in lower roughness values in a few layers (1L, 2L, 3L, and 4L). In addition, in the thin layers, with the raising of the number of carbon chains, there is more disordered the organic space then it could be creating more binding to fulfill the surface, leading to fewer pinholes in C12 and then

increased in C8, and C4. Besides, some discontinued perovskite layers can react with the ambient environment, thereby affecting the surface [22].

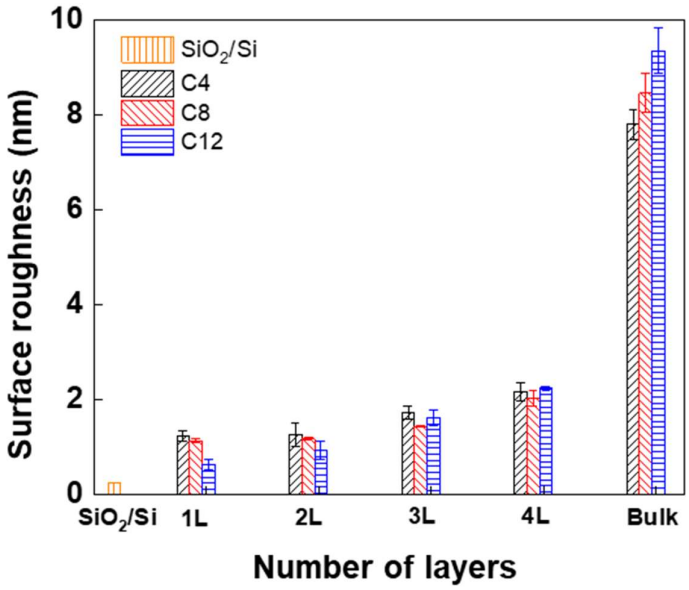

Figure 4. Surface roughness average (Ra) values of C4, C8, and C12 with single-layer (1L), bi-layer (2L), tri-layer (3L), quad-layer (4L), and bulk compared to SiO_2/Si substrate obtained at 500 nm × 500 nm areas.

2.2 Friction force measurements

After characterizing the morphology and topography, the friction properties were examined via friction force microscopy (FFM) using nanocrystalline diamond tips (ND-CTIR1S-5, NaDiaProbes, Advanced Diamond Technologies) to reduce tip wear during the contact-mode measurements. The cantilevers were calibrated in the normal [23] and lateral [24, 25] directions for the quantitative determination of normal force and lateral force. The calibration process showed a normal spring constant and lateral force sensitivity of 0.68 ± 3.79 × 10^{-3} N/m and 2.69 × 10^{-6} N/V (mean ± one standard deviation). FFM measurements were performed and repeated at least three times at

various normal forces F_n of 0 nN, 1 nN, 3 nN, 5 nN, 7 nN, and 10 nN with 100 nm scan sizes in the ambient conditions. The surface of each flake was checked after the test, and no significant surface damage was observed even at F_n = 10 nN.

3. RESULTS AND DISCUSSION

3.1 Effect of topography

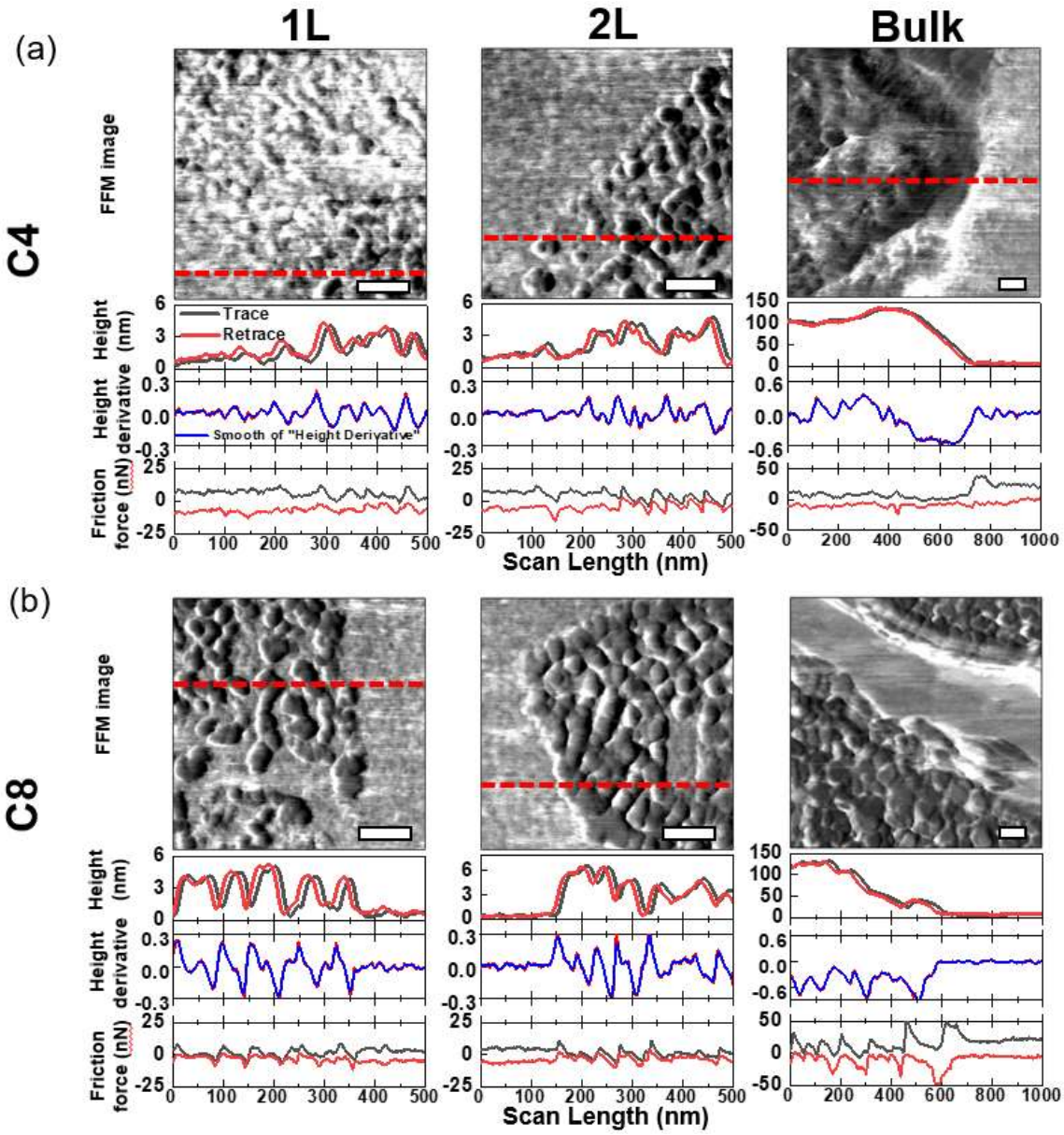

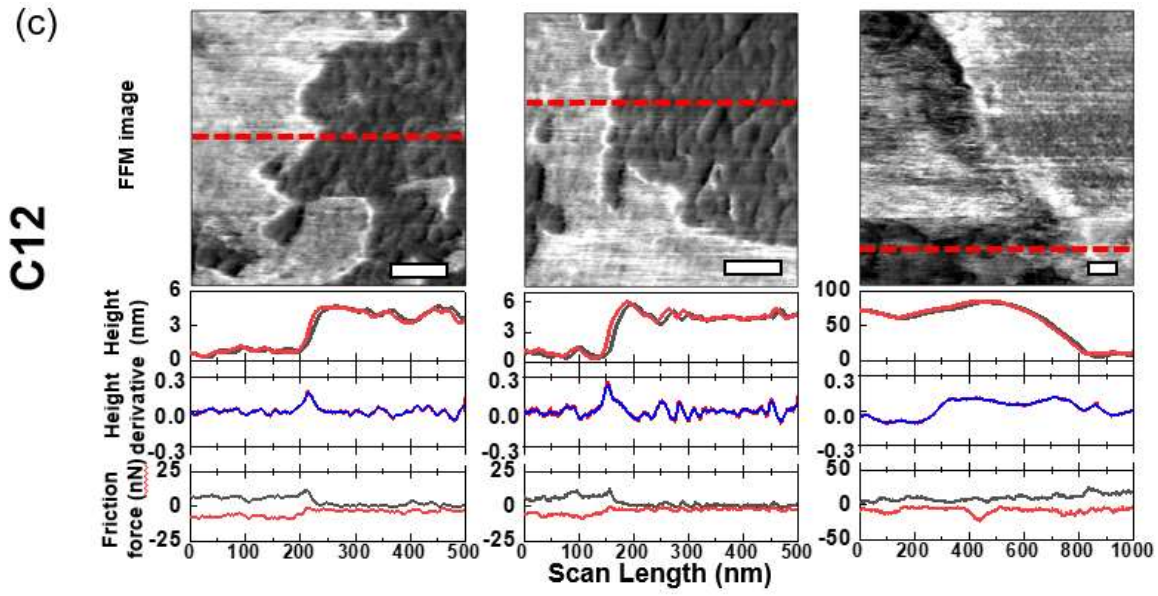

Figure 5. FFM images of 1L, 2L, and bulk with (a) C4, (b) C8, and (c) C12 were obtained from the contact mode AFM under F_n= 1 nN, the scale bar is 100 nm. In (a), (b), and (c), cross-sectional height profiles, derivative of cross-sectional height profiles, and friction loops are included. Red dash lines indicate the locations where the cross-sectional profiles and friction loops were taken.

The FFM images of 1L, 2L, and bulk with cross-sectional height profiles, height derivatives, and friction loops for C4, C8, and C12 flakes at F_n= 1 nN obtained via FFM were shown in Figure 5. The FFM images and friction loops showed that the friction of three types of 2D HOIPs for 1L, 2L, and bulk films was generally lower than that for the underlying SiO_2/Si substrate. The variation in friction fluctuation corresponded to the surface slope variation which was further estimated by taking the derivative of the cross-sectional profiles. Although the friction strongly fluctuated by the topography [26-28], the intrinsic friction of the layers was low. For example, corresponding to the topographic images and roughness mentioned above, the surface in 1L and 2L had more shape of

“island clusters” which created more slope of the surface, therefore, affecting the high fluctuation of friction loops, however, the resulting friction was still very low in all C4, C8, and C12. Also in the bulk, with the variation in friction fluctuation, the friction obtained is lower than that of the substrate. In addition, the friction of layers looked like decreasing from 1L to 2L and then increased to bulk in C4, C8, and C12. The differences in this tendency could be caused by the roughness of the surface [29]. As shown above, the roughness values increased with the rising in the number of layers and maximum for the bulk, thus, the increase of friction from 2L to bulk could be understood that, conversely, the increase of friction from 1L to 2L could be caused by other factors would be discussed below. Moreover, considering the rising of the carbon molecular chains from C4 to C12, the friction was likely gradually decreased in 1L and 2L, and slightly increased in bulk. It might be because of fewer “island clusters” on the surface of C12, then no more slope variation, and C12 gained the lowest friction in both 1L and 2L, followed by C8 and C4. The changes in the friction of bulk from C4 to C12 may also be affected by roughness given that C12 got the highest roughness value, followed by C8 and C4. Therefore, it indicated that the effect of topography on friction could not be eliminated, however, the intrinsic friction may be low.

3.2 Effect of the number layers

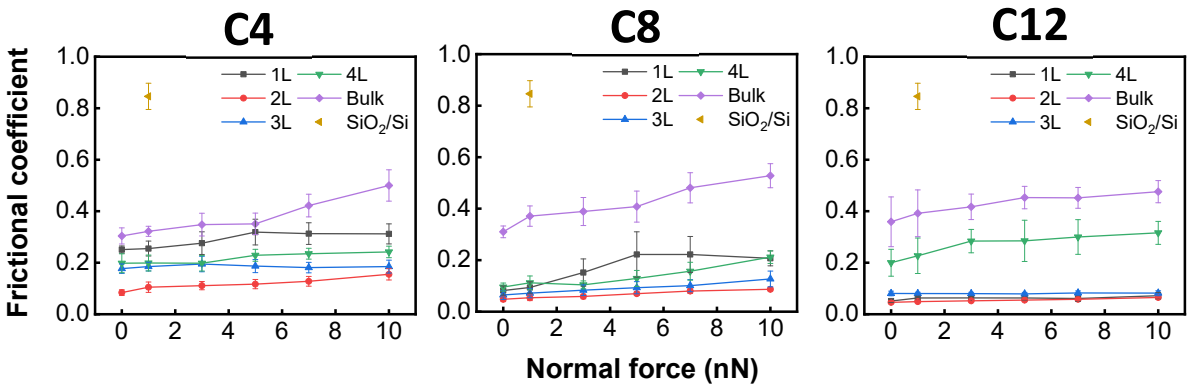

Figure 6. Normal force-dependent frictional coefficient for C4, C8, and C12 as thickness increases from 1L to bulk. The frictional coefficient was obtained at F_n= 0 nN, 1 nN, 3 nN, 5 nN, 7 nN, and 10 nN with 1L, 2L, 3L, 4L, and bulk compared to SiO_2/Si substrate.

Figure 6 showed frictional coefficient as a function of normal force for C4, C8, and C12 thin flakes at F_n= 0 nN, 1 nN, 3 nN, 5 nN, 7 nN, and 10 nN. Overall, it is worth noting that the coefficient of friction on the SiO_2/Si substrate was greater than those of the 2D HOIPs in C4, C8, and C12 (at least four times in magnitude). Besides that, the frictional coefficient increases moderately with increasing normal force. Generally, regarding the coefficient of friction of 2D HOIPs flakes, there are several factors to be considered about the mechanical origin effects or beyond the phonon properties such as adhesion [30], puckering effects [26, 29, 31], the out-of-plane elastic modulus [7, 9, 32], and phonon energy dissipation [29, 33-36]. Due to tip-substrate adhesion can influence friction [30], the average adhesion forces were performed between the tip and thin flakes for C4, C8, and C12 as thickness increases from 1L to bulk (Figure 7). It shows that there was no significant difference in adhesion between areas of different thicknesses,

therefore, the effect of adhesion, in this case, may be negligible. In previous work, it was reported about the puckering effect, where adhesion to the sliding of AFM tip induces out-of-plane deformation, leading to increased contact area and friction [29, 31]. Therefore, the thicker films with higher bending stiffness would exhibit a smaller contact area and less friction, conversely. In addition, the van der Waals force in the carbon organic chains is the weakness bonding in the structure of 2D HOIPs, therefore, under mechanical force, the shear deformation can occur [11, 20] and then affect the friction. Hence, the out-of-plane Young's modulus of the organic chains needs to be considered as a factor affecting the friction of 2D HOIP flakes. Moreover, the early studies showed that the phonon energy dissipation is one of the mainly attributed to the friction of this 2D material due to unique phonon-electron coupling properties [29, 35]. It is said that the surface layer is supposed to act as a means of transferring kinetic energy and the rates of energy dissipation are proportional to the vibrational frequency of the atoms resulting in higher friction [37]. The schematic in Figure 8 described the fundamental relationship between the layered structure of 2D HOIPs and shear deformation as well as phonon energy dissipation when the AFM tip slides on the surface. In which, L_{C4}, L_{C8}, and L_{C12} were indicated for the different organic chains; SD_{C4}, SD_{C8}, and SD_{C12} denoted the shear deformation; $V_{P,C4}$, $V_{P,C8}$, and $V_{P,C12}$ represented the phonon velocity of C4, C8, and C12, respectively. This schematic would help to clearly understand the effect of the factors on friction as detailly discussed below.

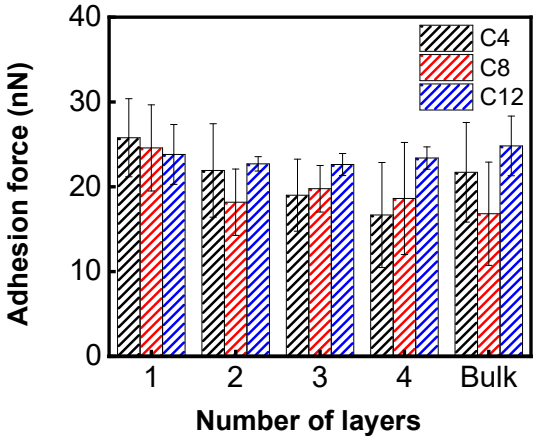

Figure 7. Average adhesion forces between the tip and thin flakes for C4, C8, and C12 as thickness increases from 1L to bulk.

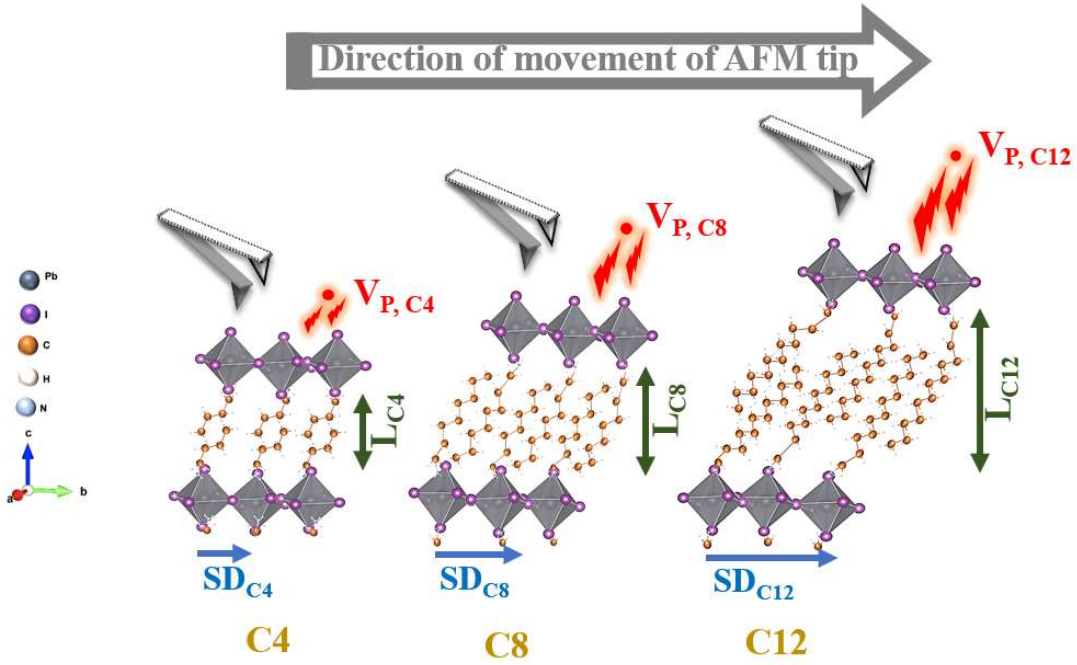

Figure 8. Schematic of shear deformation and phonon energy dissipation when the AFM tip slides on the surface of the layered 2D HOIPs with the increasing length of carbons in the organic molecular chain C4, C8, and C12. $V_{P,C4}$, $V_{P,C8}$, and $V_{P,C12}$ are the phonon velocity of C4, C8, and C12, respectively.

In terms of thickness-dependent frictional coefficient, as the thickness increased in Figure 6, the friction coefficient first decreased from 1L to 2L, and then increased to bulk for all chain lengths. It means the bulk films had the highest friction coefficient and 2L films had the lowest one (about 4 times in magnitude compared to bulk). These tendencies were consistent with the measured increased frictional coefficient of aligned contacted perovskite sheet and indium tin oxide (ITO) interfaces [6] when increasing the layer number of 2D HOIPs, except 1L films. Also, the frictional coefficient obtained in Fig. 3 is slightly higher than those values [6], which might be because of the difference in the crystal structure of the substrate. As reported [11], the shear modulus in 2D perovskite increases with a decrease in the number of layers, however, in bulk is significantly lesser compared to that of 2D HIOPs. For instance, as shown in Figure 8, if the thickness increase in all C4, C8, and C12, the shear modulus increase, then more shear deformation, thus the friction will be an increase from 1L to 4L and decrease in bulk, but the gained results from experiments was not same for 1L and bulk films. As mentioned, the bulk films have a strong interaction between the layers than the thin ones [6], thus, although the less shear modulus in bulk films, it could not be more deformation, leading to the highest and constant friction coefficient. The difference in the frictional behavior of 1L films compared to the others could be due to the puckering effect on sliding friction [29, 38]. After an AFM tip slide over the surface of 1L films which have low bending rigidity would deform out-of-plane, leading to more contact area than a higher frictional coefficient. Furthermore, as a dramatic phonon energy dissipation observed in 1L graphene [28, 36], the electron-phonon coupling in the surface of 2D HOIPs 1L films could interact more strongly, leading to more efficient dissipation and

higher friction in 1L films relative to 2L films. In general, the friction characteristics of 2D HOIPs layers to are most evident in all thicknesses from 1L to bulk films.

3.3 Effect of the organic chain length

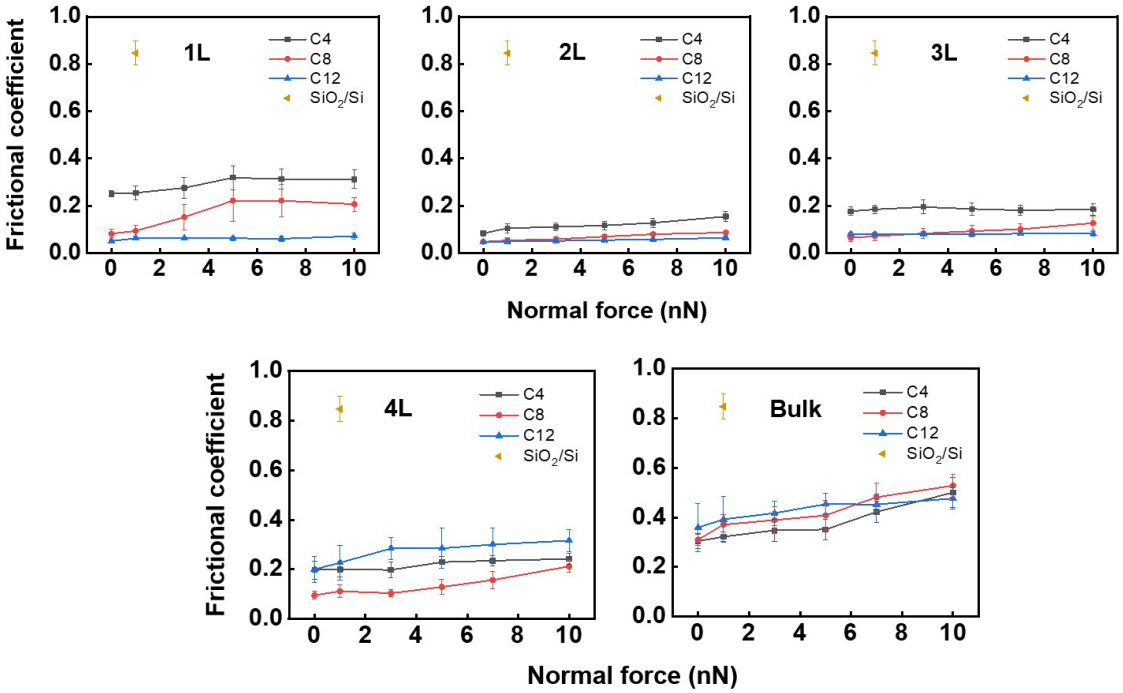

Figure 9. Frictional coefficient as a function of normal force of thin flakes 2D HOIPs, and SiO_2/Si substrate. The friction coefficients were obtained for C4, C8, and C12 at F_n= 0 nN, 1 nN, 3 nN, 5 nN, 7 nN, and 10 nN with 1L, 2L, 3L, 4L, and bulk compared to SiO_2/Si substrate.

Figure 9 was shown the effect of the organic molecular chains on the coefficient of friction for C4, C8, and C12 films. For 1L, 2L, and 3L 2D HOIPs films, the frictional coefficient gradually decreased with increasing organic molecular chain length from C4 to C12 at the same normal forces. These results can be explained by the difference in the out-of-plane elastic modulus of 2D HOIPs induced by a softening effect [7, 9, 32]. As a

larger organic molecule chain, resulting in a decrease in out-of-plane Young's modulus, hence C4 has the highest elastic modulus and C12 has the lowest one. It also corresponded to the shear deformation in Figure 8. As Young's modulus decreased, led to softer material [7], therefore, there was more deformation in shearing (increase in SD_{C4}, SD_{C8}, and SD_{C12}, respectively). These results affected the frictional behavior the frictional coefficient gradually decrease from C4 to C12 in 1L, 2L, and 3L. Several studies have shown that the velocity and lifetime of the phonon will affect the friction force [33, 34]. It has been said that increasing the van der Waals bonding between the aliphatic tails in the organic chains or the length of the organic spacers can significantly increase the phonon velocity [33]. Besides, the theory suggests that a shorter phonon lifetime corresponds to a higher friction force [35]. In the schematic in Figure 8, with the increase of organic chains ($L_{C4}<L_{C8}<L_{C12}$), the phonon velocity would be increased ($V_{P,C4}<V_{P,C8}<V_{P,C12}$), resulting in lower energy dissipation, therefore, the smallest friction coefficient in C12, followed by C8, and C4. Considering the coefficient of friction in 4L films, C12 has the highest one, followed by C4, then C8; and in bulk films, C12 also has the highest frictional coefficient, then followed by C8, and C4. It could be said that this might be due to Young's modulus decreasing to a saturation threshold with increasing chain length [7, 12]. Therefore, as the thickness of layers increases to 4L, and bulk, the total number of carbon chains increases, leading to a saturation threshold in Young's modulus, then not clearly the tendency of friction. Also, here the effect of puckering was not significant when changing the carbon chain length from C4 to C12. Generally, the length of the organic molecular chain can affect the frictional coefficient that gradually

decreases from C4 to C12 in molecularly thin 2D HOIPs layers (1L, 2L, and 3L films), and not more clearly tendency in 4L and bulk films.

4. CONCLUSIONS

4.1 Conclusions

In this work, the fundamental friction characteristics of thin flakes 2D HOIPs at the scale nano were studied. The effect of topography, effect of the number layers as well as effect of the organic chain length were quantitatively investigated through the AFM-based approaches, FFM measurement on single-, bi-, tri-, quad-layer, and bulk 2D HOIPs with three different types of organic chain C4, C8, and C12.

1. The effect of topography on nanoscale friction has been observed in the frictional behaviors according to local slope variation but the intrinsic friction is still small.
2. Frictional coefficient first decreases from single-layer to bi-layer and then increase to bulk as the same normal forces.
3. With increasing organic molecular chain length from C4 to C12, the coefficient of friction gradually decreased at the same normal forces in single-layer, bi-layer, and tri-layer. However, it is assumed that the effect of the organic chain length on friction becomes less significant as the number of layers increase.

4.2 Recommendations for the future works

Based on the limitations of this work, several commendations were made for further investigation to optimize the factors affect to the friction characteristics for the stability application. Firstly, aging effect could lead to changes in topography as well as friction, therefore, systematic research is needed to investigate the effects of aging on friction characteristics. Secondly, the study of interfacial strength and surface damage characteristics of 2D HOIPs to gain the better understanding of tribological

characteristics. Finally, inorganic layers have a greater influence on mechanical properties of 2D HOIPs than organic layers, therefore, the effect of thickness of inorganic layers on friction characteristics is necessary.

REFERENCES

[1] Sun, K.; Shen, S.; Liang, Y., Burrows, P. E; Mao, S.S and Wang, D.; Enabling silicon for solar-fuel production. *Chem. Rev.* **2014**, *114* (17), 8662-719.

[2] Fan, R.; Mi, Z. and Shen, M.; Silicon based photoelectrodes for photoelectrochemical water splitting. *Opt Express* **2019**, *27* (4), A51-A80.

[3] Turner, J.; Mann, M.; Maness, P., Kroposki, B.; Ghirardi, M.; Evans, R. and Blake, D.; Renewable hydrogen production. *International Journal Of Energy Research* **2008**, *32*, 379-407.

[4] Kim, G.; Min, H.; Lee, K. S.; Lee, D. Y. and Seok, S. I.; Impact of strain relaxation on performance of alpha-formamidinium lead iodide perovskite solar cells. *Science* **2020**, *370* (6512),108-112.

[5] Wang, H.; Ma, J. and Li, D.; Two-Dimensional Hybrid Perovskite-Based van der Waals Heterostructures. *J. Phys. Chem. Lett.* **2021**, *12* (34), 8178-8187.

[6] Bi, S.; Li, Q.; Yan, Y.; Asare-Yeboah, K.; Ma, T.; Tang, C.; Ouyang, Z.; He, Z.; Liu, Y. and Jiang, C.; Layer-dependent anisotropic frictional behavior in two-dimensional monolayer hybrid perovskite/ITO layered heterojunctions. *Phys. Chem. Chem. Phys* **2019**, *21* (5), 2540-2546.

[7] Tu, Q.; Spanopoulos, I.; Hao, S.; Wolverton, C.; Kanatzidis, M. G.; Shekhawat, G. S. and Dravid, V. P.; Out-of-Plane Mechanical Properties of 2D Hybrid Organic-Inorganic Perovskites by Nanoindentation. *ACS Appl. Mater. Interfaces* **2018**, *10* (26), 22167-22173.

[8] Tu, Q.; Spanopoulos, I.; Yasaei, P.; Stoumpos, C. C; Kanatzidis, M. G; Shekhawat, G. S. and Dravid, V. P.; Stretching and Breaking of Ultrathin 2D Hybrid Organic-Inorganic Perovskites. *ACS Nano* **2018**, *12* (10), 10347-10354.

[9] Gao, H.; Wei, W.; Li, L.; Tan, Y. and Tang. Y; Mechanical Properties of a 2D Lead-Halide Perovskite, $(C_6H_5CH_2NH_3)_2PbCl_4$, by Nanoindentation and First-Principles Calculations. *J. Phys. Chem. C* **2020**, *124*, 19204-19211.

[10] Tu. Q.; Spanopoulos, I.; Hao, S.; Wolverton, C.; Kanatzidis, M. G.; Shekhawat, G. S. and Dravid, V. P.; Probing Strain-Induced Band Gap Modulation in 2D Hybrid Organic–Inorganic Perovskites. *ACS Energy Lett.* **2019**, *4*, 796–802.

[11] Li, Q.; Bi, S.; Bu, J.; Tang, C.; Ouyang, Z.; Jiang, C. and Song, J.; Atomic Layer Dependence of Shear Modulus in a Two-Dimensional Single-Crystal Organic–Inorganic Hybrid Perovskite. *J. Phys. Chem. C* **2019**, *123*, 15251–15257.

[12] Niu, W.; Eiden, A.;Prakash, G. V. and Baumberg, J. J.; Exfoliation of self-assembled 2D organic-inorganic perovskite semiconductors. *Appl. Phys. Lett.* **2014**, *104*, 171111.

[13] Yu, S.; Liu, P. and Xiao, S.; A review of main characterization methods for identifying two-dimensional organic–inorganic halide perovskites. *Journal of materials science* **2021**, *56*, 11656-11681.

[14] Billing, D.G. and Lemmerer, A.; Synthesis, characterization and phase transitions in the inorganic-organic layered perovskite-type hybrids [(CnH2n+1NH3)2PbI4], n = 4, 5 and 6. *Acta Crystallogr B* **2007**, *63* (5), 735-47.

[15] Lemmerer, A. and Billing, D.G.; Synthesis, characterization and phase transitions of the inorganic-organic layered perovskite-type hybrids [(C(n)H(2n+1)NH3)2PbI4], n = 7, 8, 9 and 10. *Dalton Trans* **2012**, *41* (4), 1146-57.

[16] Lemmerer, A. and Billing, D.G.; Synthesis, characterization and phase transitions of the inorganic–organic layered perovskite-type hybrids [(CnH2n+1NH3)2PbI4] (n = 12, 14, 16 and 18). *New J. Chem.* **2008**, *32,* 1736-1746.

[17] Pradeesh, K.; Baumberg, J. J. and Prakash, G. V.; In situ intercalation strategies for device-quality hybrid inorganic-organic self-assembled quantum wells. *Appl. Phys. Lett.* **2009**, *95*, 033309.

[18] Stoumpos, C. C.; Cao, D. H.; Clark, D. J.; Young, J.; Rondinelli, J. M.; Jang, I. I.; Hupp, J. T. and Kanatzidis, M. G.; Ruddlesden–Popper Hybrid Lead Iodide Perovskite 2D Homologous Semiconductors. *Chem. Mater.* **2016**, *28*, 2852–2867.

[19] Dhanabalan, B.; Castelli, A.; Palei, M.; Spirito, D.; Manna, L.; Krahne, R. and Arciniegas, M.; Simple fabrication of layered halide perovskite platelets and enhanced photoluminescence from mechanically exfoliated flakes. *Nanoscale* **2019**, *11* (17), 8334-8342.

[20] Leng, K.; Fu, W.; Liu, Y.; Chhowalla, M. and Loh, K. P.; From bulk to molecularly thin hybrid perovskites. *Nature Reviews Materials* **2020**, *5*, 482–500.

[21] Leng, K.; Abdelwahab, I.; Verzhbitskiy, I.; Telychko, M.; Chu, L.; Fu, W.; Chi, X.; Gou, N.; Chen, Z.; Zhang, C.; Xu, Q.-H.; Lu, J.; Chhowalla, M.; Eda, G. and Loh, K. P.; Molecularly thin two-dimensional hybrid perovskites with tunable optoelectronic properties due to reversible surface relaxation. *Nat Mater* **2018**, *17* (10), 908-914.

[22] Ho, K.-T.; Leung, S.-F.; Li, T.-Y.; Maity, P., Cheng, B.; Fu, H.-C., Mohammed, O. F. and He, J.-H.; Surface Effect on 2D Hybrid Perovskite Crystals: Perovskites

Using an Ethanolamine Organic Layer as an Example. *Adv Mater* **2018**, *30* (46), 1804372.

[23] Hutter, J. L. and Bechhoefer, J.; Calibration of atomic-force microscope tips. *Review of Scientific Instruments* **1993**, *64*, 868.

[24] Chung, K.-H. and Reitsma, M. G.; Note: Lateral force microscope calibration using multiple location pivot loading of rectangular cantilevers. *Rev. Sci. Instrum.* **2010**, *81* (2), 026104.

[25] Tran-Khac, B.-C. and Chung, K.-H.; Quantitative assessment of contact and non-contact lateral force calibration methods for atomic force microscopy. *Ultramicroscopy* **2016**, *161*, 41-50.

[26] Tran-Khac, B.-C. and Chung, K.-H.; Operational and environmental conditions regulate the frictional behavior of two-dimensional materials. *Appl. Surf. Sci.* **2019**, *483*.

[27] Yu, C. and Wang, Q. J.; Friction anisotropy with respect to topographic orientation. *Sci. Rep.* **2012**, *2*, 988.

[28] Chen, L.; Chen, Z.; Tang, X.; Yan, W.; Zhou, Z.; Qian, L. and Kim, S. H.; Friction at single-layer graphene step edges due to chemical and topographic interactions. *Carbon* **2019**, *154*, 67-73.

[29] Zhang, S.; Ma. T.; Erdemir, A. and Li, Q.; Tribology of two-dimensional materials: From mechanisms to modulating strategies. *Materials Today* **2019**, *26*, 67-86.

[30] Waghmare, A. K. and Sahoo, P.; Adhesive friction at the contact between rough surfaces using n-point asperity model. *Inter. Jour. Engineering Science and Technology* **2015**, *18*, 463.

[31] Lee, C.; Li, Q.; Kalb, W.; Liu, X.-Z.; Berger, H.; Carpick, R. W. and Hone, J.; Frictional characteristics of atomically thin sheets. *Science* **2010**, *328* (5974), 76-80.

[32] Tu, Q.; Spanopoulos, I.; Vasileiadou, E. S.; Li, X.; Kanatzidis, M. G.; Shekhawat, G. S. and Dravid, V. P.; Exploring the Factors Affecting the Mechanical Properties of 2D Hybrid Organic-Inorganic Perovskites. *ACS Appl. Mater. Interfaces* **2020**, *12* (18), 20440-20447.

[33] Berman, D.; Erdemir, A. and Sumant, A.V.; Approaches for Achieving Superlubricity in Two-Dimensional Materials. *ACS Nano* **2018**, *12* (3), 2122-2137.

[34] Guo, P.; Stoumpos, C. C.; Mao, L.; Sadasivam, S.; Ketterson, J. B.; Darancet, P.; Kanatzidis, M. G. and Schaller, R. D.; Cross-plane coherent acoustic phonons in

two-dimensional organic-inorganic hybrid perovskites. *Nat. Commun.* **2018**, *9* (1), 2019.

[35] Z. Wei, Duan, Z.; Kan, Y.; Zhang, Y. and Chen, Y.; Phonon energy dissipation in friction between graphene/graphene interface. *Journal of Applied Physics* **2020**, *127*, 015105.

[36] Sales de Mello, S.R.; Maia da Costa, M. E. H.; Menezes, C. M.; Boeira, C. D.; Freire Jr, F. L.; Alvarez, F. and Figueroa, C. A.; On the phonon dissipation contribution to nanoscale friction by direct contact. *Sci. Rep*. **2017**, *7* (1), 3242.

[37] Ogletree, D. F.; Carpick, R. W. and Salmero, M.; Calibration of Frictional Forces in Atomic Force Microscopy. *The Review of scientific instruments* **1996**, *67*, 3298 - 3306.

[38] Filleter, T.; McChesney, J. L.; Bostwick, A.; Rotenberg, E.; Emtsev, K. V.; Seyller, Th.; Horn, K. and Bennewitz, R.; Friction and dissipation in epitaxial graphene films. *Phys. Rev. Lett.* **2009**, *102* (8), 086102.